Interlayer free – nickel doped silica membranes for desalination

A Darmawan[1,*], L Karlina[1], Y Astuti[1], Sriatun[1], D K Wang[2], J Motuzas[2], J C D da Costa[2]

[1]Diponegoro University, Department of Chemistry, Semarang 50275, Indonesia.
[2]The University of Queensland, FIM2Lab-Functional Interfacial Materials and Membranes Laboratory, School of Chemical Engineering, Brisbane Qld 4072, Australia.

*corresponding author e-mail: adi_darmawan@undip.ac.id
Tel.:+62-8222-121-9817

Abstract. This work shows for the first time the potential of nickel oxide silica membranes for desalination applications. Nickel oxide silica xerogels were synthesised via a sol–gel method including TEOS, nickel nitrate with and without addition of hydrogen peroxide. The effects of nickel addition (5% - 50 mol %) on the structure–property relationship of the silica materials were systematically studied. The membrane performance were tested as a function of feed salt concentration (0.3–3.5 wt% NaCl) and temperature (27–60 °C). The membranes which were prepared using equal sol–gel conditions to the xerogel samples showed the raised feed temperatures resulted in increased water fluxes, whilst increasing the salt concentration resulted in decreased water fluxes. The membranes with addition of hydrogen peroxide exhibited better performances than their H_2O_2 absence counterpart. The salt rejection was in excess of 90% and the maximum flux observed was 7.3 kg m^{-2} h^{-1} at 60°C for a 0.3 wt% NaCl feed concentration.

Introduction

The world is facing a global water crisis due to population growth and climate change [1]. With increasingly limited water resources, the use of infinite number of sea water becomes one choice in the provision of clean and fresh water, hence the desalination technology is one of solution[2]. Currently, approximately 43.5% of the desalination systems in the world are still using thermal technology. Membrane technology becomes an alternative instead of thermal desalination [3] because it uses less energy and produce greater water fluxes. In commercial applications, the polymeric membrane are still dominating the market despite of the polymeric membranes have some limitations, especially in their thermal and chemical stability, hence some researchers tried to find a new alternative using inorganic membranes [4-10]

There are two types of inorganic membranes that have been tested for molecular sieve application, zeolite membranes and silica membranes. In general, silica membranes are developed primarily for gas separation [11, 12]. However, some studies have shown that silica membranes coated on alumina support could reject salt ranging from 92% to 99% [8, 10, 13-15]. However, one of the main obstacles in using silica membranes for water purification is due to their hydro instability. To overcome this

problem, some researches have been done i.e. by adding the ligand and surfactant [10, 13], by carbonization a non-ligand template into a silica matrix [10, 16-18], and doping silica membrane with metal both as single metal such as cobalt [19], niobium [20], iron [21], nickel [22, 23] or binary metal such as cobalt-iron [24, 25], palladium-cobalt [26] and lanthanum-cobalt [27, 28]. Amongst these works, cobalt oxide silica membranes have been extensively examined for enhancing the hydrothermal stability, mainly for high temperature wet gas separations. Cobalt oxide silica membranes were also investigated for desalination [15, 29]. A common features of silica based membranes is an asymmetric configuration with a combination of γ-/α-alumina interlayers which their primary roles are to reduce the surface irregularities and roughness of the substrate which may cause stresses leading to film defects, cracks and generally poor membrane performance [30]. However, adding intermediate layers to the membrane fabrication process, not only increases costs but also the processing time and manual handling requirements. Recently, Elma and co-worker [29, 31] and Liu et al [32] reported the preparation of interlayer-free membranes which improved transport to high water fluxes.
In this research, it will be studied the synthesis of nickel oxide impregnated silica membranes for desalination applications as well as optimization of membrane synthesis variables against expected characters. Also, it will be assessed the performance of the resulting membrane for desalination of sea water.

Experimental Section

1. Preparation of nickel doped silica sol and xerogel

The nickel oxide silica sol was prepared similar to metal oxide silica sol methods synthesis according to the method of Darmawan et al [21] and Lin et al [15], the major difference being the use of nickel nitrate instead of iron nitrates or cobalt nitrates. Briefly, nickel oxide sols were synthesized by the hydrolysis and condensation of tetraethyl orthosilicate (TEOS, Aldrich) in absolute ethanol (EtOH) with and without 30% aqueous H_2O_2 with nickel nitrate nonahydrate ($Ni(NO_3)_2.6H_2O$). An initial molar ratio of 255 EtOH: 4 TEOS: *x* $Ni(NO_3)_2.6H_2O$: *y*H_2O_2: *z* H_2O was mixed and vigorously stirred for 3 hours in an ice-cooled bath to avoid partial hydrolysis as suggested by de Vos and Verweij [33]. The *x* molar concentration of $Ni(NO_3)_2.6H_2O$ was varied 0.2; 0.4, 1, 1.4 and 2 to give Ni/Si molar ratio of 5%, 10%, 25%, 35% and 50%. The *y* molar of H_2O_2 was varied of 0 and 9 for absence and presence of hydrogen peroxide. The *z* molar ratio of H_2O was varied to maintain the water mol ratio of 40 where the water of crystallization was taken into account. The aim of this preparation procedure was to recognize the effect of nickel content and hydrogen peroxide to character of xerogel produced. Other variables such as stirring time, drying temperature (60 °C), calcination ramp rate (2 °C/min) and a final calcination temperature (500^{o}C) were kept constant. The sol was then further prepared for characterisation.
An aliquot of each sol sample was dried in a temperature-controlled drying oven at 60 °C under normal atmospheric conditions to form a xerogel. The xerogel samples were crushed finely and calcined at temperature 500°C with ramp rates of 2°C min^{-1} in ambient pressure air and held for 2 h at the preferred temperature.

2. Membrane Synthesis

Thin membrane films were coated on macroporous alumina substrates (α-Al_2O_3 tubular support (ϕ≈97 mm), Ceramic Oxide Fabricates) via a dip-coating process with a dwell time of 2 min and a dipping and withdrawal rate of 10 cm min^{-1}. Each layer was calcined separately after dip coating at 500 °C in a temperature controlled furnace, with a hold time of 2.5 h and a ramp rate of 2 °C min^{-1}. The dip-coating and calcination procedure were repeated five times to reduce the probability of thin film defects and to obtain high quality membranes with high salt rejection

3. Characterization of nickel oxide impregnated silica membrane

Nickel doped silica membrane xerogels in powder form were characterised by using a Shimadzu IRAffinity-1 Fourier-transform infrared (FTIR) spectrometer with a Pike MIRacle attenuated total reflectance accessory (ATR-FTIR) at wavelength range 400–4000 cm^{-1}. Deconvolution of the FTIR spectra was performed using the Fityk computer program with Gaussian peak fitting as the preferred

curve. The same number of peaks was used in all the spectral peak fitting. The half width at half maximum (HWHM) was fixed for each peak, while the peak position was allowed to change slightly to realize qualified fitting. The peak area for silanol at 950 cm^{-1} was normalized against the peak area of the siloxane bridges at 1080 cm^{-1}. The gravimetric analyses of the nickel doped silica membrane xerogels were performed on a Shimadzu thermogravimetric analyser TGA-50 using air flow rate of 60 mL min^{-1} and heating rate 2°C min^{-1}. Nitrogen adsorption analysis was performed at 77 K and 1 bar using Micromeritic TriStar 3020 instrument of samples degassed under vacuum for >6 h at 150°C. The specific surface area was determined from the Brunauer, Emmett and Teller (BET) method and total pore volume was taken from the last point of the isotherm. Adsorption average pore width (4V/A by BET) methods was taken to determine the average pore sizes. The porosity (ϵ) can be calculated from this volume of adsorbed nitrogen, according to [34]

$$\epsilon(\%) = \frac{V_p}{V_p + (\frac{1}{\rho})} \times 100\% \quad (1)$$

in which V_p is the pore volume (ml/g), and ρ is the density of the solid phase (g/ml). A skeletal density of 2.2 g/cm^3 was used for amorphous calcined silica [34]. The pore volume is calculated from the adsorbed gas volume [ml(STP)/g, at 1 atm and 0°C] assuming ideal gas behaviour and taking the density of liquid nitrogen, ρ = 0.808 g/ml, which yields

$$V_p = V_{ads} \times 1.547 \times 10^{-3} \quad (2)$$

with V_p in ml liquid N_2/g and V_{ads} in ml (STP)/g.

4. Membrane performance

Nickel oxide impregnated silica membrane performance for the desalination of sea water is tested by measuring the produced water flux and rejected salt concentration. The salt concentration and temperature of the feed water are kept constant. The membrane was assembled into a filter set-up for desalination experiments. The membrane was assembled into a classical pervaporation set-up for desalination experiments as shown in Figure 1 according to the method of Elma [31]. The membrane was immersed in a tank containing saline feed solution. The membrane was blocked at one end and connected to a cold trap (immersed in liquid nitrogen) and vacuum pump operating at 1.5 kPa at the other end. The feed solutions were prepared with sodium chloride (NaCl) dissolved in deionised water with concentrations ranging from 0.3 and 3.5 wt% and temperature was varied from room temperature, 40 °C and 60 °C. The feed solution was under constant recirculation to prevent concentration polarisation on the contact membrane side.

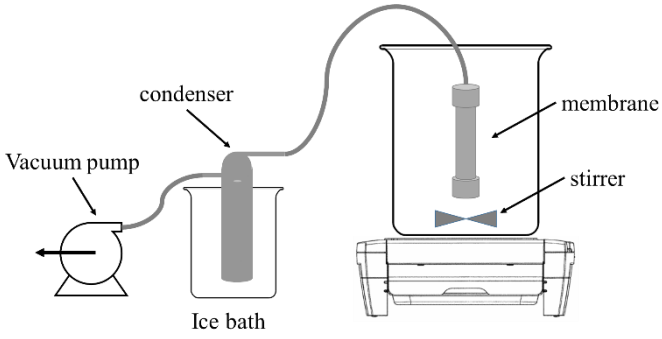

Figure 1. A membrane desalination set up

The water flux, F (kg $m^{-2}h^{-1}$), was determined based on the equation $F=\frac{m}{A\Delta t}$, where m is the mass of permeate (kg) retained in the container, A is the surface-active area (m^2) of the membrane and Δt is the time measurement (h). The salt rejection, R (%), was calculated as $R=\frac{C_f - C_p}{C_f} \; x \; 100\%$, where C_f and C_p are the feed and permeate concentrations of salt (wt%). The salt concentrations were correlated to conductivities of the retentate and permeate solutions determined by a conductivity meter.

Results and Discussion

1. Nitrogen Adsorption

The physical and textural properties of the nickel doped silica xerogels were studied by nitrogen sorption which provides important qualitative information regarding the microstructure of the resulting molecular sieving membranes. The adsorption-desorption isotherms are shown in Figure 2. The BET surface areas, total pore volumes and average pore diameters are summarised in Figure 3. In porous inorganic membrane, the pore volume generally provides an indication of the membrane flux while the pore size is related with the separation of molecules or purity. In general, pore sizes with diameters greater than 50 nm are classified as macroporous; between 2 and 50 nm are mesoporous and smaller than 2 nm are microporous.

For all samples with addition of hydrogen peroxide, the isotherms of nickel doped silica xerogels resulted in microporous materials with a type I isotherm as indicated by a very strong initial adsorption at very low partial pressures ($P/P_o < 0.2$) followed by saturation and are thus characteristic of microporous materials, which produced the low surface area (~330-390 m^2 g^{-1}), total pore volume (0.17-0.21 cm^3 g^{-1}) and the average pore radius remained similar at around 2.1 nm (±0.05 nm). This consistency is similar with the result of iron doped [21] and cobalt doped silica membranes [15, 32, 35]. Although pore volumes and surface areas varied depending upon the Ni/Si ratio.

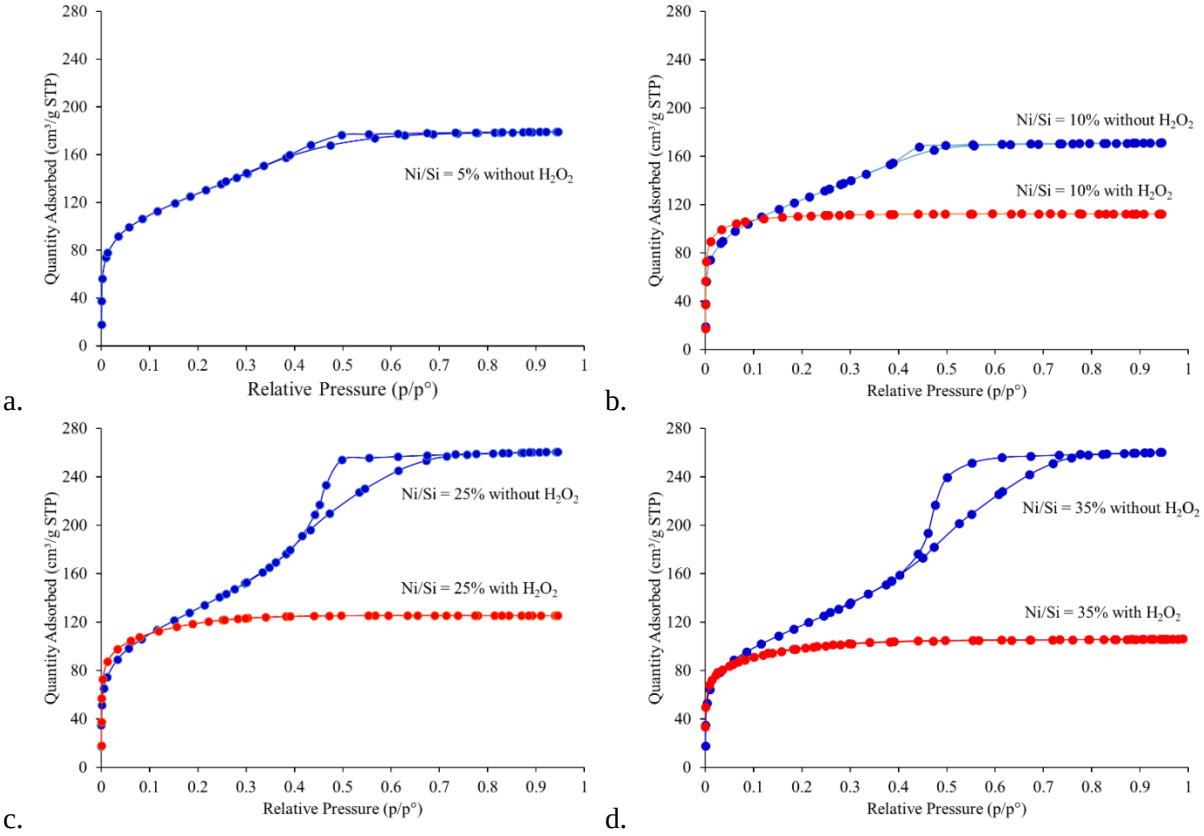

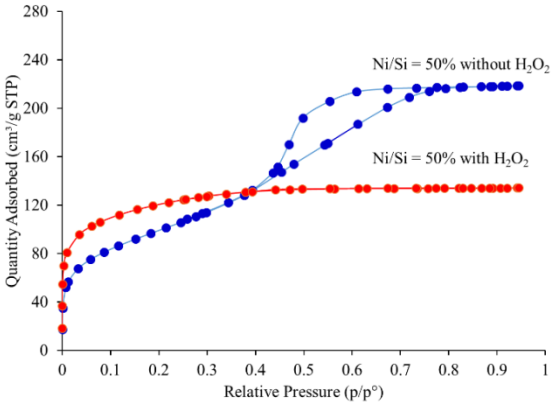

e.

Figure 2. Nitrogen adsorption–desorption isotherms the nickel doped silica xerogels (a) Ni/Si=5% (b) Ni/Si=10% (c) Ni/Si=25% (d) Ni/Si=35% (e) Ni/Si=50%

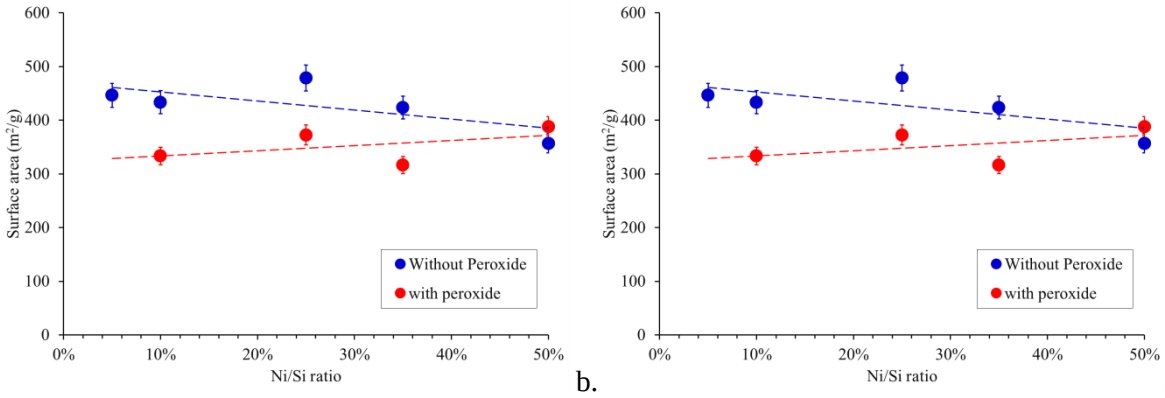

a. b.

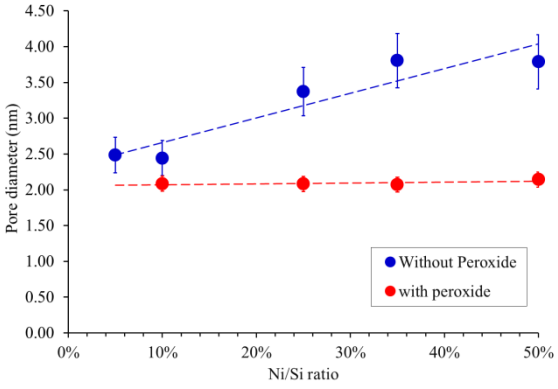

c.

Figure 3. Surface properties of bulk nickel doped silica xerogels (a) surface area (b) pore volume (c) pore diameter

It can be seen that the pore structures tend to shift to mesoporous region as Ni/Si molar ratio increases. This result differs from other studies showing that the addition of metal oxides lowers surface area and pore volume [21] as the metal oxide generally have a low surface area as compared to polymeric silica although similar observations are typically observed in cobalt-silica materials [36]. This result is suggesting that nickel oxide opposes the densification of the silica matrix by stiffening the silica aggregates against the collapse during drying. However, the amorphous silica is still dominantly responsible for the textural properties of the nickel doped oxide silica matrix. It appears to be expected that the amorphous silica structure is enveloped the nickel oxide particles.

Interestingly, in the absence of hydrogen peroxide, a significant structural re-arrangement is observed where the nickel doped silica xerogels tended to form mesoporous materials with a higher adsorption

saturation capacity above 0.4 p/p° and a hysteresis with a smooth inflection indicating a type IV isotherm. The surface area, pore volume and pore diameter increases of 30% up to twice. The absence of hydrogen peroxide in the nickel doped silica samples contributed to mesoporous formation (average pore radius > 2 nm), lead to higher surface area (>400 $m^2 \cdot g^{-1}$) and total pore volume (up to 0.4 $cm^3 \cdot g^{-1}$). It is interesting to observe in Figure 2 that the hysteresis loops due to escalation in multilayer adsorption are increasing by the increase of the nickel which confirming the broadening of the pore sizes. Moreover, when nickel/silica ratio reached 25 wt%, it is clearly detected that the isotherm profiles are truly type IV isotherms and mesoporous as evidenced by their large extent of hysteresis near p/p°=0.5 indicating the occurrence of capillary condensation.

The position of inflection is an increasing function of the pore diameter [37]. Since by increase of nickel content, the position of inflection shifted to a higher value of p/p°, the pore sizes should be increase. Significantly large pore diameters reached the values close to 3.8 nm. The change of porosity should correspond to the decrease in selectivity of the membrane. This result clearly indicating that the structural modifications in the template xerogel are directly attributed to the hydrogen peroxide molecules which has a far greater impact on the resultant structure than originally thought. The results above strongly suggest that the hydrogen peroxide facilitates the formation of polymeric silica species during the early stage of the sol-gel process and the condensation occurs preferentially between silanol groups located on monomers or the ends of polymers as occurring on acid-catalysed sol-gel reaction. Conversely, by absence of H_2O_2, the preferred reaction sites for condensation are on the most deprotonated silanol bonds of the Q^3 Si atoms [38] and condensation reaction via the monomer–cluster growth pathway [19] which tends to produce mesoporous silica materials.

The change of textural properties of these silica based matrices can also be rationalized by the change of pH of the sol as H_2O_2 depresses the pH in 2 digit below their H_2O_2 absence counterpart. Such changes in the sol pH have been well known had a dramatic effect on the microstructure of the silica matrices as reported elsewhere [29, 38, 39]. When the sol is acidified by adding the H_2O_2, hydrolysis reaction is promoted which long chains of siloxane bonds, forming a weakly branched polymer. This type of bond can densify relatively easily upon drying and calcination forming a mesh like structure where the connected interchain apertures form pores of 2-4Å [40-42].

By absence of hydrogen peroxide, the nickel doped silica sol pHs were between (4-5) which is higher than the isoelectric point boundary (pH 1–3) of the silica species [43]. At this instance, the silanol species are expected to be all deprotonated participating in the polycondensation reaction generating a significant amounts of silica monomers constantly forming and reforming, in a process known as Ostwald ripening, allowing the structure to settle to its most thermodynamically favoured configuration with a large concentration of highly condensed species (e.g., siloxane bridges) and thereby creating a highly branched silica network.

Interestingly, it was found that the solution pH shifted to a more acidic region by the increasing nickel content in the solution. This pH shift was found to be systematic from pH 4.62 (Ni/Si = 5%), 4.25 (Ni/Si = 10%), 4.23 (Ni/Si = 25%), 4.14 (Ni/Si = 35%) to pH 4.05 (Ni/Si = 50%). But conversely, it lead the pore structure to be more mesoporous. This fact is in contrary to what had been believed that the increase of acidity causes the silica matrix structure to more microporous [29, 38, 39]. This fact strengthen the idea which has been described above that the nickel oxide inhibits densification of the silica matrix.

Although pH decreased (acidity increased), the increasing of mesoporosity can be justified that although the pHs of nickel doped silica solution remained quite close to, but they were still above the isoelectric point, at the which there is no electrostatic particle- particle repulsion [29] hence the effect of pH was not more dominant than the effect of dispersion of metal ions in solution.

Compared with the elements in the same transition group (Group VIII), indeed, the nickel is less acidic than iron and cobalt. The acidity sequence is Fe > Co > Ni. Iron is more acidic as the solution containing 3+ ion tends to have pH's in the range from 1 to 3 whereas the solutions containing 2+ ions have higher pH's which typically around 4-5. The ions that have smaller ionic radius will be less acidic and as nickel ionic radius is smaller than cobalt, its acidity is lower than cobalt. This explains why the

iron doped silica was very acidic (pH<2) and had a microporous structure as reported by Darmawan [21] whilst the cobalt doped silica with the addition of peroxide had a pH of 3 and produced microporous structure as reported by Lin [15]. While at higher pH, cobalt doped silica produced mesoporous structures [29]. However, it seems there is no definite relationship between pH ranges with microporosity or mesoporosity silica matrix resulted. Elma and co-workers [39] reported the silica xerogel without the addition of transition metals produced a solution with a pH = 7 and the resulting structure was mesoporous. It appears that textural properties of silica matrix was the resultant effect of metal, hydrogen peroxide and the pH.

As can be seen in Figure 4, the porosity increases with increasing nickel content as calculated from the volume of adsorbed nitrogen, as expressed in Equation (1). Hence the silica matrix structure with the higher nickel content will be more polymerized and more branched thus more porous. The porosities for sample with absence of H_2O_2 are always higher than their presence of H_2O_2 counterpart. In the presence of H_2O_2, the structures would be expected to pack very well and form structures with very low porosities.

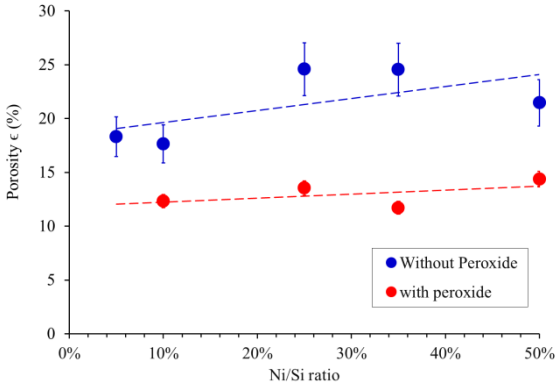

Figure 4. Effect of Ni/Si molar ratio on porosity

2. Infrared Spectroscopy analysis

Figures 5(a) and 3(b) show the IR spectra of xerogel samples between wave number 650 and 1450 cm^{-1}. It is observed that regardless of the Ni/Si molar ratio variation, the presence or absence of H_2O_2, the IR spectra of the xerogel samples remained almost persistent.

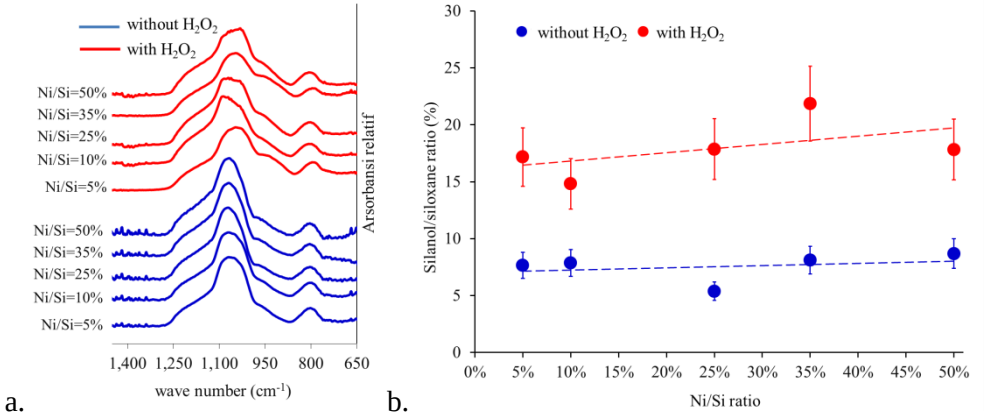

a. b.

Figure 5. (a-left) FTIR spectra of samples as a function of Ni/Si molar ratio where (i) 5%, (ii) 10%, (iii) 25% (iv) 35% (v) 50% (vi) 10% with H_2O_2 (vii) 25% with H_2O_2 (viii) 50% with H_2O_2, (b-right) Silanol and siloxane ratio as of samples as a function of Ni/Si molar ratio

These FTIR results suggest that all nickel doped silica xerogels had similar surface chemical. These results suggest that no significant variation of silica functional groups was reached by introduction of nickel. The formation of the silanol and siloxane groups was still governed by the silica hydrolysis and condensation reactions. It has been widely reported that the dissolution of metal species in the sol–gel process produces metal nanoparticles in the porous structure of silica [24, 44].

The bands observed are conventionally found in silica materials which include the bands at 800 cm^{-1} and 1070 cm^{-1} with a shoulder near 1200 cm^{-1} corresponding to different modes of siloxane stretching bonds (Si-O-Si): symmetric and asymmetric, respectively. The shoulder in the region of 960 cm^{-1} is assigned to the stretching vibration of Si–OH [45, 46]. At the absence of hydrogen peroxide, the peak of Si–O band (1070 cm^{-1}) position has been observed to be similar in the very narrow range (1068-1070 cm^{-1}), however in the presence of hydrogen peroxide there was a significant shift at the asymmetric Si-O band from 1086 cm^{-1} (Ni/Si=10% + H_2O_2), 1070 cm^{-1} (Ni/Si=10% + H_2O_2) to 1032 cm^{-1} (Ni/Si=10% + H_2O_2), indicating that Si–O–M (M is the metal atom) hetero-linkages were probably formed [47]. If the number of Si–O–M linkages increases, the number of Si atoms in Si-O-Si linkages decrease and consequently in the silanol groups at the surface will increase. Hence the intensity ratio of the 960 cm^{-1} band to 1070 cm^{-1} band could be used to measure relative heterogeneity of nickel and silica.

To understand further the effect of water in the formation of functional groups of the iron oxide silica matrices, the FTIR spectra in Figure 5a were deconvoluted using a Gaussian method and the result is showed in Figure 5b. The deconvolution allows the calculation of a silanol (~960 cm^{-1}) to siloxane (~1070 cm^{-1}) ratio. Regardless the presence and absence of hydrogen peroxide, the trend is consistent in the sense that the silanol/siloxane ratio is constant by increasing the nickel/silica ratio with concern to the error bar. This result suggests that the nickel oxide is not chemically bound to the silica, and remains as particles embedded into the silica matrix. The existence of nickel does not give any effect to either accelerate or retard the condensation reaction of silanol into siloxane.

Remarkably, the nickel doped silica xerogels with the presence of H_2O_2 show the silanol/siloxane ratio which is always higher than their same Ni/Si content counterpart. These results clearly indicate that the lower silanol concentrations, or likewise the higher siloxane bridge concentrations were achieved with the xerogels prepared with addition of hydrogen peroxide. Hence, it could be strongly proposed that the presence of H_2O_2 actually inhibits the condensation reaction and stabilize the presence of silanol from the hydrolysis reaction. These barriers lead to insufficient energy to drive the reaction to full condensation. As silanols are pendulous functional groups which not chemically inter-linked to other silica structures like siloxane bridges, therefore silanols are recognized as unreserved structures. Hence, silanols have the proclivity to freely interpenetrate one another which is known as weakly branched systems [48]. It was explained that weak branching combined with limited condensation during film formation promotes dense packing and low pore volume [49].

By absence of H_2O_2, the synthesis conditions are more favourable towards the condensation reactions which is proved by the lower silanol/siloxane ratio. This then lead to interconnect the siloxane structures with one another which is known as strongly branched systems. The increase in the siloxane bridges is parallel connected with any increase of surface area and pore volume which accord with the fractal theory.

An additional point of importance here is that the production of high siloxane bridges in silica membranes has been reported to oppose hydro-instability [50, 51]. Therefore, since the nickel doped silica xerogels with absence of H_2O_2 produces more siloxane groups, it should be more hydro-stable.

3. Thermal Analysis

Typical thermograms and weight change derivatives obtained for nickel oxide silica xerogels are shown in Figures 6 (a)(b) and Figure 7 respectively.

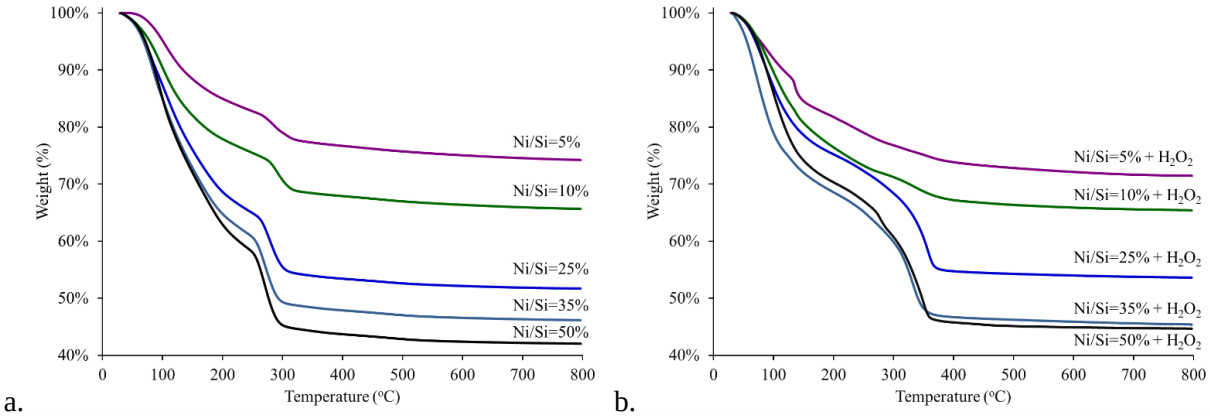

Figure 6. Mass loss curves of samples as a function of Ni/Si molar ratio (a-left) without addition of H_2O_2 and (b-right) with addition of H_2O_2

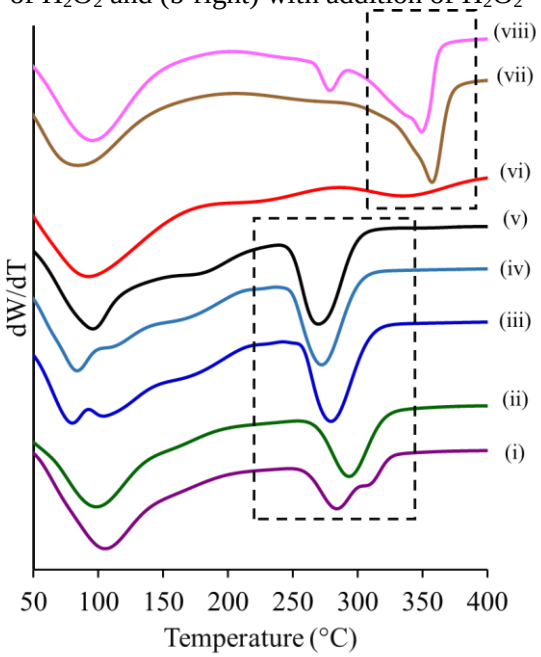

Figure 7. Differential of the TGA for samples prepared with varying Ni/Si molar ratios where (i) 5%, (ii) 10%, (iii) 25% (iv) 35% (v) 50% (vi) 10% with H_2O_2 (vii) 25% with H_2O_2 (viii) 50% with H_2O_2

The weight reduction increased gradually by increasing the amount of nickel. These results strongly suggest that the addition of iron is affecting the sol-gel processes. All the samples displayed a two stage decomposition behaviour i.e. two major weight loss regions, (i) in the temperature range of 35-245°C (ii) in the range of 245°–800°C are seen. From 80-120^{o}C, the weight loss is generally caused by the loss of free (not chemically bound) H_2O and ethanol molecules. The sharp decrease in weight is related with the increase of Ni/Si molar ratio, suggesting that an increasing nickel content results in increased H_2O within the uncalcined xerogel matrix. As nickel in $Ni(NO_3)_2$ is surrounded by 6 H_2O molecules consequently increasing the nickel content in the sol-gel will equally increase the amount of water in the sample. The decline in the mass observed at 150-350°C corresponds to the completion of dehydration and the dehydroxylation due to the condensation of the OH groups in the silica particles [52, 53], and the oxidation of the residual carbons (from ethanol and reaction by-product) which may be trapped inside the silica network. This trend remains until the next weight loss peaks between 150-350^{o}C, whereby total decreasing of weight correspond with increasing nickel content. This may be

considered as nitrate decomposition, related to NO and NO_2 deformation which may take place around 245-350 °C.

Comparing the Figure 6 a and b, it can be found that generally with the same amount of nickel content, the quantity of weight loss is almost similar. This result indicates that the contribution of weight loss is dominated by the nickel nitrate decomposition. Conversely, the weight loss contours are different. In the nickel doped silica with absence of H_2O_2, there is a constant curve decline up to 250 °C, while by the presence of H_2O_2, the curves decrease sharply to 150 °C and from there on become slighter. In contrast, with absence of H_2O_2, the curves decrease sharply at a temperature of 250-325 °C. This may occur since the addition of H_2O_2 lead the silica structure to be more bulky to facilitate the deformation process run faster at lower temperatures. Meanwhile, with presence of H_2O_2, the silica matrix structure is denser and thus require a higher temperature to deform.

The trend of mass loss as a function of the nickel to silica ratio and presence of H_2O_2 was further analysed as per Figure 6. It is evident that the major losses occurred up to 150°C, which is mainly attributed to physisorbed water and ethanol retained in the silica matrix. As mentioned above that nickel ion is surrounded by 6 H_2O molecules which further aiding in mass loss. The samples with higher nickel content contain larger amounts of fluid in their structure (per unit weight of the sample). Therefore, this structure has to be more porous than the structures of samples with lower nickel content. This conclusion is in accordance with results from the nitrogen adsorption measurements in which samples with increasing nickel content show an increase in porosity as shown in Figure 4.

For nickel doped silica in the absence of H_2O_2, the bottom highlighted box inside the Figure 7 shows that by increasing of nickel content, the deformation temperatures decrease which marked by the peak shift to the lower temperature. This result is in line with the FTIR results which show there is no bond between nickel oxide and silica hence the increase of nickel content in silica matrix should reduce the deformation temperature.

Interestingly, the top highlighted box inside the Figure 7 shows the deformation temperatures of nickel doped silica xerogels in the absence of H_2O_2 are always higher than their H_2O_2 presence counterpart. This could be understood because the absence of H_2O_2 nickel doped silica xerogels produce denser structures as described from the results of surface morphology which is marked by smaller pore diameters. Whilst the presence of H_2O_2 nickel silica generates more open structure which causes the nitrate group to decompose more easily.

4. Desalination measurements

Membrane performance is commonly evaluated based on the permeating water flux and the salt rejection. Figure 8 and 9 shows the performance of the nickel doped silica as a function of salt concentration and temperature. In general, all the nickel doped silica membranes produced moderate water fluxes up to 7.5 kg m^{-2} h^{-1} with good salt rejections reaching values up above 90% in all testing condition. This series of membranes show that the desalination performance does not follow gradual sequence as function of nickel content. However, the membranes with presence of H_2O_2 always demonstrated higher performance in salt rejection but lower in water flux compared to their H_2O_2 absence silica membrane counterpart in all testing condition. For all membranes, greater permeating water flux was observed at temperatures by increasing of temperature. However, there is a decreasing in salt rejection as the temperature raised. The loss of performance due to increasing of temperature is comparable to the results reported for cobalt silica membrane [15, 29]. Raising the temperature of the salt solution permitted for an increasing of the vapour pressure hence increasing the driving force for the water permeation.

The flux dropped when the membrane were tested in higher NaCl concentration, indicating some effect of NaCl within the larger pores of the membrane. The increased driving force of NaCl across the membrane leads to this flux increase. The separation performance of the Ni/Si=10% and 25% membrane with presence of H_2O_2 showed the highest rejection was possible at 0.3 wt% of around 99.9%. This decreased slightly when NaCl concentration at 3.5% to around 97.5%. The ability to desalinate to potable standards of below 0.05 wt% was achievable by all membranes at 0.3 wt% feed. At 3.5 wt% feed simulating seawater, for Ni/Si=10% membrane with presence of H_2O_2, the NaCl

concentration in the permeate reduced to 0.04 wt% which is below to the 0.05 wt% drinking water standard. It is likely that Ni/Si=10% silica membrane with presence of H_2O_2 could transport seawater to potable standards in a single pass. When compared to the performance of the cobalt oxide silica membranes [15], the water fluxes produced by the nickel membranes are much higher (300%) although the salt rejections are slightly lower. This result suggests that the absence of γ-alumina interlayer gave a significant increase of water fluxes.

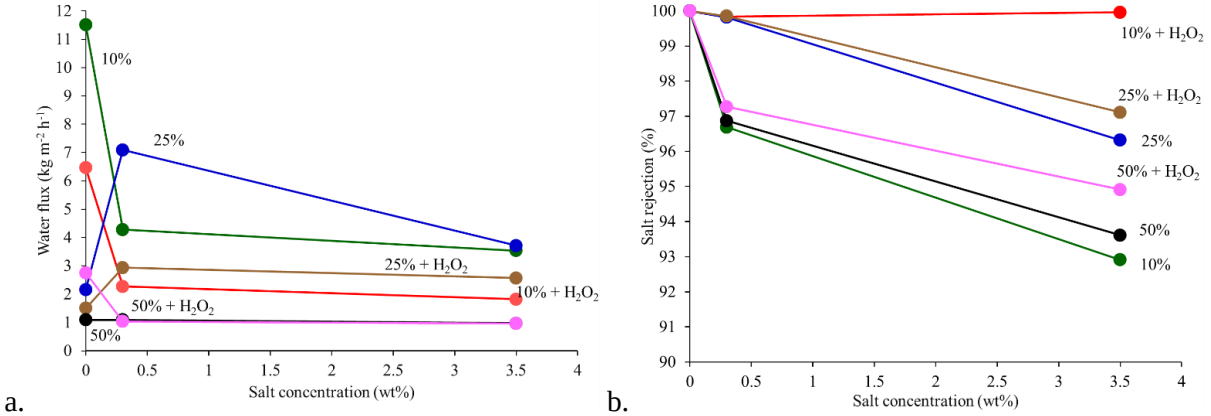

a. b.

Figure 8. Membrane desalination performance as function of salt concentration toward (a) water flux (b) salt rejection at room temperature

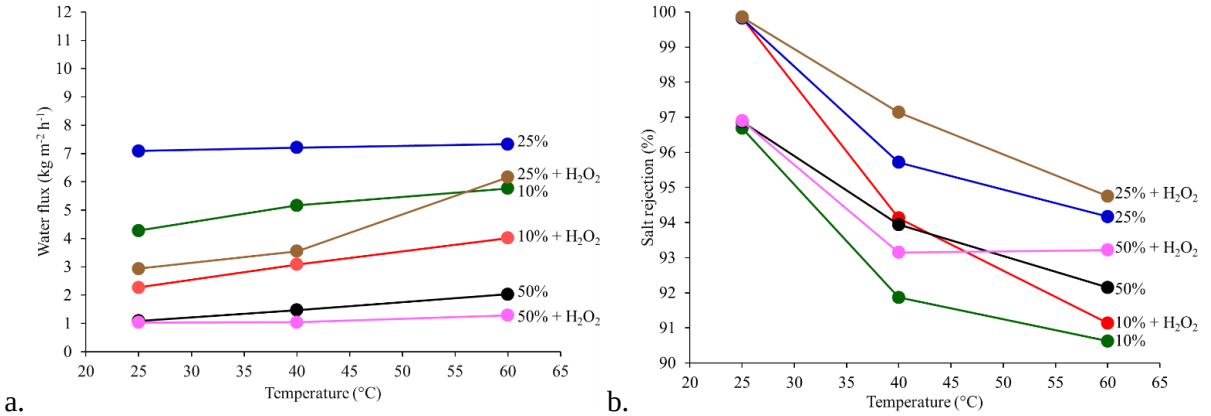

a. b.

Figure 9. Membrane desalination performance as function of temperature toward (a) water flux (b) salt rejection at 0.3% salt concentration

It seems obviously there is a close relationship between the membrane performance and the surface area as recognised by N_2 sorption as shown in Table 1. For example, in a given fixed salt concentration 0.3 wt% and temperature 25°C, the water flux values are (4.3, 2.3); (7.1, 2.9) and (1.1, 1.03) kg m^{-2} h^{-1} whereas the surface area value are (433, 333); (478, 372) and (356, 388) m^2/g for the pair of (10%, 10%+H_2O_2); (25%, 25% + H_2O_2) and (50%, 50% + H_2O_2) membranes, respectively. This behaviour also likely directly related to the pore volume and average pore size of the nickel doped silica membranes. It has been well known that the pore volume controls the water flux while the pore diameter controls the sieving. The salt rejection is generally controlled by the pore size where large pores cause pore wetting due to the hydrophilic properties of silica and consequently low rejection whilst small pores deliver high salt rejection.

Table 1 obviously show that the nickel doped silica membranes resulted in average pore sizes measured between 2.08 and 3.8 nm. Actually, these average pore sizes are too big to conduct a molecular sieving to separate water molecules from solution but usually the thin films have smaller pore sizes than their bulk counterparts. Although the original chemistry that govern silica polymeric growth and gelation are principally the same for films as bulk gels, however there are other factors that influence structural evolution in films [43, 54] such as due to non-equivalent gelation and drying

conditions. If all nickel doped silica pores were all mesoporous (pore diameter >2 nm), the membranes should not be able to reject any hydrated salt ions. As the desalination results in this work show that there is a salt rejection, it can be said that the nickel doped silica silica membranes were dominated by a vast majority of pore sizes less than the size of hydrated salt ions (Na^+ : d_k = 7.2 Å and Cl^- : d_k = 6.6 Å) and above water molecule (d_k = 2.6 Å).

The nitrogen sorption isotherms results (Figure 2) strongly show that there were much structure differences between the absence and presence of H_2O_2 and also the influence of nickel content to the silica matrix. As mentioned above, the presence of H_2O_2 was expected to consolidate the silica matrix uniformly, establish the silanol stability and increasing the silica network dominated by microporous structures. Oppositely, the absence of H_2O_2 makes the pore arrangement of silica structure to be more open and accelerate the formation of siloxane bond. The fact that the xerogels exhibit mesoporous structure when the membrane produces molecular sieving with high salt rejection is an interesting finding. It is often mentioned that xerogels displaying a microporous region produce a selective membrane while xerogels featuring a mesoporous component do not produce this same effect. However, this work shows that it is possible to produce a selective thin film with a xerogel exhibiting a mesoporous component. There are some explanations for these experimental results. First, the average pore size and pore volume determined by sorption analysis do not provide the tortuosity of the material. Second, the sorption analysis is conducted on powdered xerogels which may have different structures to the final membrane. Third, as the membrane thin layer having a thickness of 150-200 nm, the pores overlapped or stratified each other that led to the downsizing of the filtration channel because the underneath pores is covered by upper pores.

Conclusions

The nickel doped silica xerogels and membranes were prepared using sol–gel method. The effect of nickel content ranging from 5% to 50 wt% into silica matrix was investigated for the physical and chemical properties of xerogels followed by membrane morphology and desalination performance. The findings clearly indicate that the nickel oxide content and in the silica matrix and the existence of H_2O_2 have a significant effect on the resultant silica matrix. The absence of H_2O_2 made the silica structure to be more open hence increased the surface area, pore volume and average pore size where the presence of H_2O_2 made the silica structure to be denser and close which marked by the decrease of surface area, pore volume and average pore size. No observable changes in the silica functional groups were found, thus suggesting no significant variation of silica functional group formation as a function of nickel oxide content. Large weight losses were associated with OH groups or H_2O molecules derived from the decomposition of iron nitrate nonahydrate in addition to solvents (ethanol) and organics (R groups from TEOS). Furthermore, nitrate decomposition under heat treatment led to NO and NO_2 formation, further contributing to weight losses. In other words, increasing the Ni/Si molar ratio likewise increases the weight losses. By increasing of nickel content in silica matrix, the surface morphology parameters such as surface area, pore volume and average pore size increased. This result is counterintuitive as the increase in nickel oxide content should decrease the total surface area since metal oxide particles have low surface area than polymeric silica structures, these results strongly suggest that the nickel oxides played a beneficial role in opposing the silica structure collapse.

The nickel doped silica membranes showed good salt rejection (>90%) for all testing temperatures and salt concentration. Water fluxes and salt rejection varied depending on the concentration of nickel oxide in the silica film, feed salt concentration and temperature. Nickel doped silica membrane with absence of H2O2 possessed larger pore sizes which yielded higher fluxes but lower salt rejection compared to their H2O2 presence counterpart.

References

[1] C.J. Vörösmarty, P. Green, J. Salisbury, R.B. Lammers, Global Water Resources: Vulnerability from Climate Change and Population Growth, Science, 289 (2000) 284-288.

[2] K.V. Reddy, N. Ghaffour, Overview of the cost of desalinated water and costing methodologies, Desalination, 205 (2007) 340-353.
[3] N. Voutchkov, Desalination – water for the next generation, Filtration & Separation, 42 (2005) 14-25.
[4] L. Cot, A. Ayral, J. Durand, C. Guizard, N. Hovnanian, A. Julbe, A. Larbot, Inorganic membranes and solid state sciences, Solid State Sciences, 2 (2000) 313-334.
[5] T. Tsuru, Inorganic Porous Membranes for Liquid Phase Separation, Separation & Purification Reviews, 30 (2001) 191-220.
[6] J. Wang, T. Tsuru, Cobalt-doped silica membranes for pervaporation dehydration of ethanol/water solutions, Journal of Membrane Science, 369 (2011) 13-19.
[7] M.M. Teoh, T.S. Chung, Membrane distillation with hydrophobic macrovoid-free PVDF-PTFE hollow fiber membranes, Separation and Purification Technology, 66 (2009) 229-236.
[8] G.-T. Lim, H.-G. Jeong, I.-S. Hwang, D.-H. Kim, N. Park, J. Cho, Fabrication of a silica ceramic membrane using the aerosol flame deposition method for pretreatment focusing on particle control during desalination, Desalination, 238 (2009) 53-59.
[9] N. Misdan, W.J. Lau, A.F. Ismail, Seawater Reverse Osmosis (SWRO) desalination by thin-film composite membrane—Current development, challenges and future prospects, Desalination, 287 (2012) 228-237.
[10] M.C. Duke, S. Mee, J.C.D. da Costa, Performance of porous inorganic membranes in non-osmotic desalination, Water Research, 41 (2007) 3998-4004.
[11] G.Q. Lu, J.C. Diniz da Costa, M. Duke, S. Giessler, R. Socolow, R.H. Williams, T. Kreutz, Inorganic membranes for hydrogen production and purification: A critical review and perspective, Journal of Colloid and Interface Science, 314 (2007) 589-603.
[12] J. Yang, J. Chen, Hydrophobic modification and silver doping of silica membranes for H2/CO2 separation, Journal of CO2 Utilization, (2013).
[13] S. Wijaya, M.C. Duke, J.C. Diniz da Costa, Carbonised template silica membranes for desalination, Desalination, 236 (2009) 291-298.
[14] Z. Xie, M. Hoang, T. Duong, D. Ng, B. Dao, S. Gray, Sol–gel derived poly(vinyl alcohol)/maleic acid/silica hybrid membrane for desalination by pervaporation, Journal of Membrane Science, 383 (2011) 96-103.
[15] C.X.C. Lin, L.P. Ding, S. Smart, J.C. Diniz da Costa, Cobalt oxide silica membranes for desalination, Journal of Colloid and Interface Science, 368 (2012) 70-76.
[16] M.C. Duke, J.C.D. da Costa, D.D. Do, P.G. Gray, G.Q. Lu, Hydrothermally Robust Molecular Sieve Silica for Wet Gas Separation, Advanced Functional Materials, 16 (2006) 1215-1220.
[17] M.C. Duke, J.C.D. da Costa, G.Q. Lu, C. Malde, P.G. Grayyy, Hydrothermal Stability Analysis of Carbonised Template Molecular Sieve Silica Membranes, in: C. Fell (Ed.) 2004 ECI Conference on Separations Technology VI, The Berkeley Electronic Press, Kingsher Resort, Fraser Island, Queensland, Australia, 2006.
[18] M.C. Duke, J.C. Diniz da Costa, G.Q. Lu, M. Petch, P. Gray, Carbonised template molecular sieve silica membranes in fuel processing systems: permeation, hydrostability and regeneration, Journal of Membrane Science, 241 (2004) 325-333.
[19] D. Uhlmann, S. Liu, B.P. Ladewig, J.C. Diniz da Costa, Cobalt-doped silica membranes for gas separation, Journal of Membrane Science, 326 (2009) 316-321.
[20] V. Boffa, J.E. ten Elshof, R. Garcia, D.H.A. Blank, Microporous niobia-silica membranes: Influence of sol composition and structure on gas transport properties, Microporous and Mesoporous Materials, 118 (2009) 202-209.
[21] A. Darmawan, S. Smart, A. Julbe, J.C. Diniz da Costa, Iron Oxide Silica Derived from Sol-Gel Synthesis, Materials, 4 (2011) 448-456.
[22] Y.H. Ikuhara, H. Mori, T. Saito, Y. Iwamoto, High-Temperature Hydrogen Adsorption Properties of Precursor-Derived Nickel Nanoparticle-Dispersed Amorphous Silica, Journal of the American Ceramic Society, 90 (2007) 546-552.

[23] M. Kanezashi, T. Fujita, M. Asaeda, Nickel- Doped Silica Membranes for Separation of Helium from Organic Gas Mixtures, Separation Science and Technology, 40 (2005) 225-238.
[24] A. Darmawan, J. Motuzas, S. Smart, A. Julbe, J.C. Diniz da Costa, Binary iron cobalt oxide silica membrane for gas separation, Journal of Membrane Science, 474 (2015) 32-38.
[25] A. Darmawan, J. Motuzas, S. Smart, A. Julbe, J.C. Diniz da Costa, Temperature dependent transition point of purity versus flux for gas separation in Fe/Co-silica membranes, Separation and Purification Technology, 151 (2015) 284-291.
[26] B. Ballinger, J. Motuzas, S. Smart, J.C. Diniz da Costa, Palladium cobalt binary doping of molecular sieving silica membranes, Journal of Membrane Science, 451 (2014) 185-191.
[27] B. Ballinger, J. Motuzas, C.R. Miller, S. Smart, J.C. Diniz da Costa, Nanoscale assembly of lanthanum silica with dense and porous interfacial structures, Scientific Reports, 5 (2015) 8210.
[28] B. Ballinger, J. Motuzas, S. Smart, J.C. Diniz da Costa, Gas permeation redox effect on binary lanthanum cobalt silica membranes with enhanced silicate formation, Journal of Membrane Science, 489 (2015) 220-226.
[29] M. Elma, D.K. Wang, C. Yacou, J. Motuzas, J.C. Diniz da Costa, High performance interlayer-free mesoporous cobalt oxide silica membranes for desalination applications, Desalination, 365 (2015) 308-315.
[30] A.J. Burggraaf, Chapter 8 Fundamentals of membrane top-layer synthesis and processing, in: A.J. Burggraaf, L. Cot (Eds.) Membrane Science and Technology, Elsevier, 1996, pp. 259-329.
[31] M. Elma, D.K. Wang, C. Yacou, J.C. Diniz da Costa, Interlayer-free P123 carbonised template silica membranes for desalination with reduced salt concentration polarisation, Journal of Membrane Science, 475 (2015) 376-383.
[32] L. Liu, D.K. Wang, D.L. Martens, S. Smart, J.C. Diniz da Costa, Interlayer-free microporous cobalt oxide silica membranes via silica seeding sol–gel technique, Journal of Membrane Science, 492 (2015) 1-8.
[33] R.M. de Vos, H. Verweij, Improved performance of silica membranes for gas separation, Journal of Membrane Science, 143 (1998) 37-51.
[34] R.S.A. De Lange, Microporous Sol–Gel Derived Ceramic Membranes for Gas Separation, in, University of Twente, The Netherlands, 1993.
[35] C. Yacou, S. Smart, J.C. Diniz da Costa, Long term performance cobalt oxide silica membrane module for high temperature H2 separation, Energy & Environmental Science, 5 (2012) 5820-5832.
[36] D.L. Martens, D.K. Wang, J. Motuzas, S. Smart, J.C.D. da Costa, Modulation of microporous/mesoporous structures in self-templated cobalt-silica, Scientific Reports, 5 (2015) 7970.
[37] K.-K. Kang, H.-K. Rhee, Synthesis and characterization of novel mesoporous silica with large wormhole-like pores: Use of TBOS as silicon source, Microporous and Mesoporous Materials, 84 (2005) 34-40.
[38] C.J. Brinker, Hydrolysis and condensation of silicates: Effects on structure, Journal of Non-Crystalline Solids, 100 (1988) 31-50.
[39] M. Elma, C. Yacou, J. Diniz da Costa, D. Wang, Performance and Long Term Stability of Mesoporous Silica Membranes for Desalination, Membranes, 3 (2013) 136.
[40] W.J. Elferink, B.N. Nair, R.M. de Vos, K. Keizer, H. Verweij, Sol-Gel Synthesis and Characterization of Microporous Silica Membranes: II. Tailor-Making Porosity, Journal of Colloid and Interface Science, 180 (1996) 127-134.
[41] B.N. Nair, J.W. Elferink, K. Keizer, H. Verweij, Preparation and Structure of Microporous Silica Membranes, J Sol-Gel Sci Technol, 8 (1997) 471-475.
[42] R. Leboda, E. Mendyk, V.A. Tertykh, Effect of medium pH on hydrothermal treatment of silica gels (xerogels) in an autoclave, Materials Chemistry and Physics, 43 (1996) 53-58.
[43] C.J. Brinker, G.W. Scherer, Sol-Gel Science: The Physics and Chemistry of Sol-Gel Processing, Academic Press, Inc, San Diego, 1990.

[44] D. Uhlmann, S. Smart, J.C. Diniz da Costa, H2S stability and separation performance of cobalt oxide silica membranes, Journal of Membrane Science, 380 (2011) 48-54.
[45] A. Bertoluzza, C. Fagnano, M. Antonietta Morelli, V. Gottardi, M. Guglielmi, Raman and infrared spectra on silica gel evolving toward glass, Journal of Non-Crystalline Solids, 48 (1982) 117-128.
[46] A. Duran, C. Serna, V. Fornes, J.M. Fernandez Navarro, Structural considerations about SiO2 glasses prepared by sol-gel, Journal of Non-Crystalline Solids, 82 (1986) 69-77.
[47] S. Araki, Y. Kiyohara, S. Imasaka, S. Tanaka, Y. Miyake, Preparation and pervaporation properties of silica-zirconia membranes, Desalination, 266 (2011) 46-50.
[48] B.B. Mandelbrot, Fractals: form, chance, and dimension, WH Freeman San Francisco, 1977.
[49] C.J. Brinker, A.J. Hurd, K.J. Ward, Fundamentals of Sol-Gel Thin Film Formation, in: J.D. Mackenzie, D.R. Ulrich (Eds.) Ultrastructure Processing of Advanced Ceramics, Wiley, New York, 1988, pp. 223-240.
[50] R. Igi, T. Yoshioka, Y.H. Ikuhara, Y. Iwamoto, T. Tsuru, Characterization of Co-Doped Silica for Improved Hydrothermal Stability and Application to Hydrogen Separation Membranes at High Temperatures, Journal of the American Ceramic Society, 91 (2008) 2975-2981.
[51] T. Tsuru, R. Igi, M. Kanezashi, T. Yoshioka, S. Fujisaki, Y. Iwamoto, Permeation properties of hydrogen and water vapor through porous silica membranes at high temperatures, AIChE Journal, 57 (2011) 618-629.
[52] J.M. Kim, S.M. Chang, S.M. Kong, K.-S. Kim, J. Kim, W.-S. Kim, Control of hydroxyl group content in silica particle synthesized by the sol-precipitation process, Ceramics International, 35 (2009) 1015-1019.
[53] J.C. Diniz da Costa, G.Q. Lu, V. Rudolph, Y.S. Lin, Novel molecular sieve silica (MSS) membranes: characterisation and permeation of single-step and two-step sol–gel membranes, Journal of Membrane Science, 198 (2002) 9-21.
[54] C.J. Brinker, G.C. Frye, A.J. Hurd, C.S. Ashley, Fundamentals of sol-gel dip coating, Thin Solid Films, 201 (1991) 97-108.

Acknowledgments
A. Darmawan, Y. Astuti and Sriatun gratefully acknowledge financial support from Diponegoro University via the Research for International Scientific Publications Award (Number: 315-04/UN7.5.1/PG/2015). Linda Karlina specially thanks for FIM2lab at the University of Queensland for their support for all experimental work.